Investigation of MOVPE-grown zincblende GaN nucleation layers on 3C-SiC/Si substrates

Lok Yi Lee[1, a], Martin Frentrup[1], Petr Vacek[1,2], Fabien C-P Massabuau[1], Menno J Kappers[1], David J Wallis[1,3], and Rachel A Oliver[1]

[1] Department of Materials Science and Metallurgy, University of Cambridge, 27 Charles Babbage Road, Cambridge, CB3 0FS, United Kingdom

[2] Institute of Physics of Materials & CEITEC IPM, Academy of Sciences of the Czech Republic, Žižkova 22, 61600 Brno, Czech Republic

[3] Centre for High Frequency Engineering, University of Cardiff, 5 The Parade, Newport Road, Cardiff, CF24 3AA, United Kingdom

[a] Corresponding author: lyl24@cam.ac.uk

Abstract

Cubic zincblende (zb-)GaN nucleation layers (NLs) grown by MOVPE on 3C-SiC/Si substrates were studied to determine their optimal thickness for subsequent zb-GaN epilayer growth. The layers were characterised by atomic force microscopy, X-ray diffraction and scanning transmission electron microscopy. The as-grown NLs, with nominal thicknesses varying from 3 nm to 44 nm, consist of small grains which are elongated in the [1-10] direction, and cover the underlying SiC surface almost entirely. Thermal annealing of the NLs by heating in a H_2/NH_3 atmosphere to the elevated epilayer growth temperature reduces the substrate coverage of the films that are less than 22 nm thick, due to both material desorption and the ripening of islands. The compressive biaxial in-plane strain of the NLs reduces with increasing NL thickness to the value of relaxed GaN for a thickness of 44 nm. Both the as-grown and annealed NLs are crystalline and have high zincblende phase purity, but contain defects including misfit dislocations and stacking faults. The zb-GaN epilayers

grown on the thinnest NLs show an enhanced fraction of the wurtzite phase, most likely formed by nucleation on the exposed substrate surface at elevated temperature, thus dictating the minimum NL thickness for phase-pure zb-GaN epilayer growth.

Keywords:

A1. Atomic force microscopy; A1. Nucleation; A1. X-ray diffraction; A3. Metalorganic vapor phase epitaxy; B1. Nitrides; B2. Semiconducting gallium compounds

1. Introduction

III-nitrides based on the zincblende (zb) crystal structure can offer a potential solution to the 'green gap' problem, due to the absence of internal electric fields [1], which affect the commonly used c-plane wurtzite (wz) crystal structure and result in the quantum-confined Stark effect [2]. Moreover, zb-GaN has a smaller bandgap than wz-GaN by ~ 200 meV [3] and hence zb-InGaN quantum wells require lower indium content to achieve green wavelengths compared with equivalent non-polar or semi-polar InGaN quantum wells.

Heteroepitaxial growth of zb-GaN has been achieved by molecular beam epitaxy (MBE) [4,5,14,15,6–13] and metal-organic vapour-phase epitaxy (MOVPE) [16–24] on substrates such GaAs(001) and 3C-SiC/Si(001). In the case of zb-GaN MOVPE growth, a two-step growth method is commonly employed where a thin nucleation layer (NL) grown at a relatively low temperature ensures the wetting of the substrate, a two-dimensional growth mode and a high phase purity of the zb-GaN epilayer grown subsequently at increased temperatures. Optimised NL growth temperatures between 490 °C and 575 °C and epilayer growth temperatures between 800 and 950 °C have been reported for zb-GaN MOVPE [16–23]. Although the optimisation of a low-temperature NL is of paramount importance for zb-

GaN MOVPE growth, only two studies so far have been dedicated to it [21,22]. Wu *et al.* [21] reported on the effect of NL thickness on the morphology and phase purity of zb-GaN epilayers grown on 3C-SiC/Si(100) substrates. They found that a GaN epilayer grown on a 20 nm-thick NL consists of individual large grains with a high (~ 50%) wurtzite content. In contrast, coalesced GaN layers with higher zb phase purity (> 80 %) were grown on 40 nm- and 60 nm-thick NLs. Xu *et al.* [22] studied the effect of NL growth conditions (deposition temperature, rate and time) and annealing time (at 820 ºC) on the NL morphology and surface coverage, as well as the quality of subsequent zb-GaN epilayers grown on GaAs(001) by MOVPE. Although the results of this investigation were underreported, the authors concluded that the wurtzite content of the zb-GaN epilayer increased if the substrate coverage by the (annealed) NL was incomplete.

A two-step growth method has also been used for MBE growth of zb-GaN on GaAs(001) where the low-temperature NL prevented the excessive desorption and nitridation of the GaAs substrate [8]. However, the use of a low-temperature NL is not critical for MBE growth on thermally stable substrates, as Daudin *et al.* [10] succeeded in growing high quality zb-GaN directly on 3C-SiC/Si(001), provided that the growth rate was low and the temperature less than 700 ºC.

It is clear from the discussion above that there is need for a detailed investigation on low-temperature NLs for zb-GaN MOVPE growth. Thus, in this study, we determine an optimal GaN NL thickness for subsequent zb-GaN epilayer growth on 3C-SiC/Si(001) substrates with a 4° or 2° miscut, by considering the substrate coverage of as-grown and thermally annealed NLs, strain in the NL and epilayer's phase purity. For this, both as-grown and annealed NLs and subsequent thicker epilayers were characterised by atomic force microscopy (AFM), X-

ray diffraction (XRD), Nomarski optical microscopy and cross-sectional high-resolution scanning transmission electron microscopy (HR-STEM).

2. Materials and Methods

The GaN NLs were grown by MOVPE in a 6 × 2'' Thomas Swan close-coupled showerhead reactor on ~ 2 × 2 cm^2 pieces of 150 mm diameter 3C-SiC/Si substrates provided by Anvil Semiconductors Ltd. The substrates consisted of ~ 3 μm thick layer of CMP-polished 3C-SiC grown on a 1000 μm thick Si(001) wafer with either a 4° or 2° miscut towards the [110] in-plane direction. 3C-SiC/Si substrates have the advantage of a small lattice mismatch with zb-GaN of 3.4% at room temperature [25] and being available in large diameters of up to 150 mm at present. Trimethylgallium (TMG) and ammonia (NH_3) were used as Ga and N sources, and hydrogen was used as the carrier gas. The quoted growth temperatures were determined using emission-corrected optical pyrometry, while growth rates were measured using in-situ three wavelength reflectance transients with the relevant optical constants provided by LayTec.

The GaN NLs were grown at ~ 600 ºC on co-loaded 4° and 2º miscut substrates with nominal GaN layer thicknesses of 3 nm, 6 nm, 11 nm, 22 nm and 44 nm, as calculated from the growth time at a constant rate of 0.3 nm s^{-1}, which was determined separately from a thicker NL test structure. The annealed NLs were prepared by ramping the as-grown NLs to the epilayer growth temperature of 885 °C and immediate cooling, all taking place in an atmosphere of NH_3 and H_2. To determine the optimal NL thickness, a set of 500 nm-thick epilayer samples was grown on NLs with different thicknesses on the 4° miscut substrate. The growth conditions of the epilayers included a substrate temperature of 885 °C, an input

gas flow V/III-ratio of 150 and a growth rate of 0.5 nm s^{-1}. We have previously shown that such growth conditions led to zb-GaN layers with high phase purity [26].

The surface morphologies were measured using a Bruker Dimension Icon atomic force microscope (AFM) in PeakForce mode for the NLs, and in tapping mode for the thicker epilayers. ScanAsyst-Air-HR and RTESP-300 probes from Bruker Nano Inc. with nominal tip radii of 2 nm and 8 nm were used for PeakForce and tapping modes, respectively. The fast scan direction for all the samples imaged was along the [110] miscut direction. The topographic data obtained from the AFM were analysed using the free software package WSxM [27]. The image height (H) is the height range from black to white in the AFM images, while the root mean square (rms) surface roughness (R) is defined as $\sqrt{\frac{1}{n}\sum_{i=1}^{n} z_i^2}$, where n is the number of pixels in the AFM scan and z_i is the height at a pixel. Both H and rms R are stated below each AFM scan.

Two-dimensional fast Fourier transforms (2D-FFT) of the AFM scans were used to quantify the typical sizes of the surface features along [110] and [1-10], which correspond to directions parallel and perpendicular to the miscut direction of the substrates. A 2D-FFT filter was applied to each of the 500 × 500 nm^2 AFM scans, and the intensity profile was extracted from the centre of the 2D-FFT pattern in the [110] and [1-10] directions. The intensity profile typically followed a Gaussian distribution curve, from which the full width at half maximum (FWHM) was obtained. The reciprocal of ½-FWHM gives a measure of the average feature size along [110] and [1-10], defined as $f_{[110]}$ and $f_{[1\text{-}10]}$ respectively. This procedure was repeated for four different areas on the surface of each sample, and the four measurements were averaged. The standard error of the mean from the four measurements was used to define the accuracy of our measurements. The substrate coverage of the NLs was calculated

from 500 × 500 nm^2 AFM scans using the software package Gwyddion [28], where the grains were selected using the 'mark grains by threshold' function and setting a height threshold which is typically ~ 25% of H.

X-ray diffraction (XRD) measurements were performed on two diffractometers with Cu-Kα sources (λ = 1.54056 Å). Reciprocal space maps were measured with a PANalytical Empyrean diffractometer equipped with a two-bounce hybrid monochromator, 1/4° primary beam slit, and a PIXcel solid-state area detector; while ω-2θ measurements were performed on a Philips X'pert diffactometer consisting of a 4-crystal Bartels monochromator, an adjustable crossed slits collimator, and a gas-proportional detector. The relative amounts of material deposited for NLs of the various thicknesses were deduced from the integrated intensities of the 002 zb-GaN and SiC reflections measured by $\omega 2\theta$-scans [25]. As for strain analysis, the 2θ Bragg-angle of the 002 zb-GaN reflection for each (001)-oriented GaN NL was determined by a Pseudo-Voigt fit and was used to calculate the out-of-plane lattice constant. Using the lattice constant a = 4.50597(38) Å for nominally unstrained zincblende GaN [25], the out-of-plane strain ε_z was determined and the biaxial in-plane strains ε_x were obtained using the relation $\varepsilon_z = -2 \times (C_{12}/C_{11}) \times \varepsilon_x$ [25], where C_{11} = 293 GPa and C_{12} = 159 GPa are the elastic constants of zb-GaN [3]. An alternative approach to determine the in-plane strain, which involves measuring the in-plane lattice parameter (directly) from the off-axis reflections, turned out to be too inaccurate, due to the weak peak intensities of the thin GaN NL samples. The phase purity of the epilayers was determined from the integrated intensities of the 113 zb-GaN and 1-103 wz-GaN reflections extracted from reciprocal space maps, using the method described previously [26].

Cross-sectional TEM samples were prepared using mechanical polishing, dimple grinding, and precision ion polishing with Ar^+ ions. High-resolution scanning transmission electron microscopy (HR-STEM) was performed on the samples using a FEI Titan^3 operated at 300 kV to characterise the crystallinity and phase of the NLs. Nomarski optical microscopy revealed the surface structure of the epilayer set of samples.

3. Results

3.1. As-grown NLs

The crystallinity of the as-grown NLs are revealed by XRD $\omega 2\theta$-scans of the 002 zb-GaN and SiC reflections. A typical intensity profile of such a scan is shown in Figure 1, which was obtained from the 6 nm thick as-grown NL grown on the 4° miscut substrate. The scans show that the NLs are crystalline with zincblende GaN (001) orientation. Reciprocal space maps of the nearby 10-11 wz-GaN reflection (not shown) reveal no significant intensity above the noise level, which suggests that the wurtzite phase is absent or only present in concentrations below the detection limit.

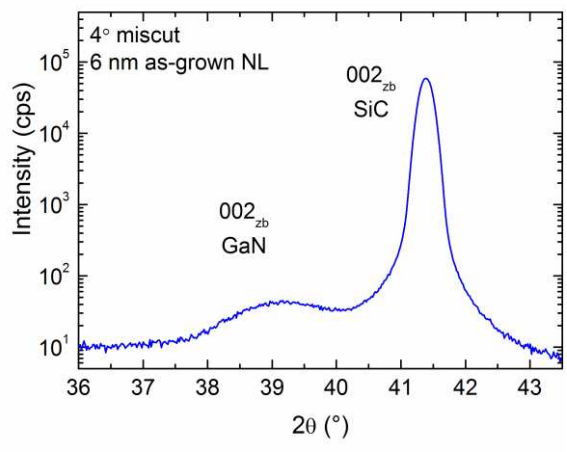

Figure 1 Intensity profile of the XRD $\omega 2\theta$-scan of the 002 zb-GaN and SiC reflections for the 6 nm as-grown NL grown on 4° miscut substrate.

The variation in surface morphology of the zb-GaN NLs with layer thickness for the as-grown set of samples is shown in the 500 × 500 nm^2 AFM height scans in Figure 2. The surface morphology of all the NLs is characterised by coalesced islands elongated along the [1-10] direction. As the NL thickness increases from 3 nm to 44 nm, the AFM scans show that these surface features become slightly larger in both [110] and [1-10] directions, while the substrate coverage remains nearly complete.

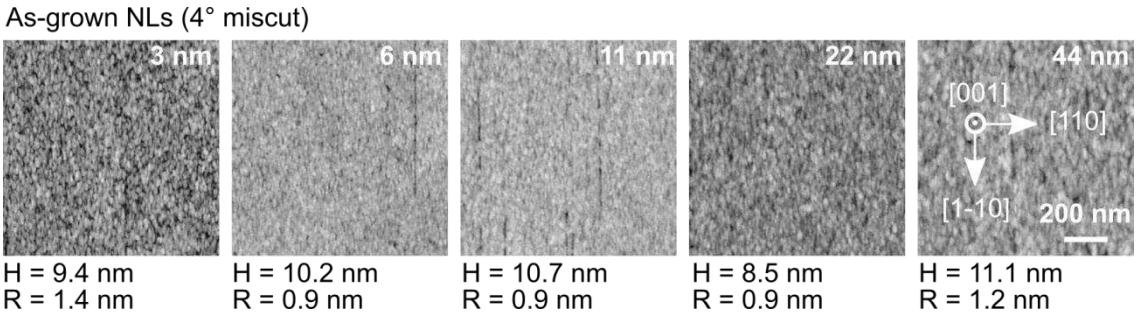

Figure 2 AFM height scans of the set of as-grown GaN NLs with different thicknesses revealing the surface morphology. The height (H) and rms roughness (R) are stated below each AFM scan.

The feature sizes in the [110] and [1-10] directions ($f_{[110]}$ and $f_{[1\text{-}10]}$) of the as-grown NLs on the 4° miscut substrate were quantified using the 2D-FFT method, and the results are shown by the filled circles and squares in Figure 3. The range of feature sizes in the [110] direction varied from 25 nm to 40 nm, while in the [1-10] direction the features are larger at between 35 nm and 70 nm. With increasing NL thickness, both $f_{[110]}$ and $f_{[1\text{-}10]}$ of the as-grown NLs increase slightly. The lateral diffusion rate is expected to be limited at the low temperature of NL growth. Therefore with increasing deposition, the material attaches to the sides of the nucleated islands to result in an increase in average feature size in [110] and [1-10] directions. Subsequently, as the islands impinge on each other, they coalesce to result in even larger $f_{[110]}$ and $f_{[1\text{-}10]}$. Therefore, the AFM data shows that the NLs are deposited as islands

which grow in size laterally and coalesce with increasing material deposition, suggesting a three-dimensional Volmer-Weber type growth mode [29] in agreement with earlier MBE growth studies on GaAs(001) [9] and 3C-SiC/Si(001) [10].

The effect of the substrate miscut on the NL morphology was studied by comparing the feature size along the two in-plane directions for the NLs grown on 4° and 2° miscut substrates. These are denoted by the filled and open circles respectively in Figure 3. The data shows that the differences in feature sizes between the two miscuts are small and within the error bars of the measurements, indicating that miscut does not have an influence on size and shape of the islands.

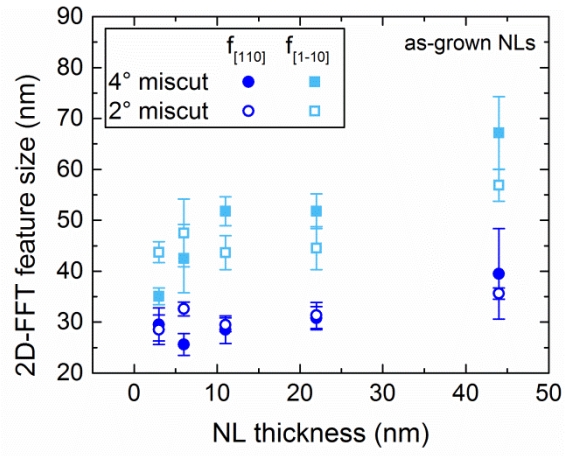

Figure 3 Feature sizes of the as-grown NLs grown on 4° (filled) and 2° (open) miscut substrates in the [110] (circle) and [1-10] (square) directions, as calculated by the 2D-FFT method.

The characteristic morphology of surface features elongated in the [110] direction of the GaN NLs was also found in thicker zb-GaN epilayers grown on similar NLs [26]. The shape of such features was explained to be the result of anisotropic diffusion on the low-symmetry top monolayer of (001) GaN lattice, with the [110] and [1-10] directions going across and along

the potential valleys of the GaN surface, respectively. A similar mechanism likely controls the morphology of the nucleation layers. We note that for the epilayer samples, $f_{[110]}$ range from 0.6 µm to 1.3 µm, and $f_{[1\text{-}10]}$ from 1.0 to 4.8 µm, which are significantly larger than the feature sizes of the NL samples. These differences in the scale are probably caused by the lower NL growth temperature, leading to shorter diffusion lengths.

3.2. Annealed NLs

The effect of an anneal treatment at the epilayer growth temperature of 885 °C on the as-grown set of NLs is revealed by the 500 × 500 nm^2 AFM height scans in Figure 4. Similar to the as-grown NLs, the surface morphology of the annealed NLs consists of features elongated in the [1-10] direction. As the NL thickness increases from 3 nm to 44 nm, the surface coverage of the substrate increases as the features become larger in both [110] and [1-10] directions and impinge on each other. It is evident that there is a reduction in surface coverage for the 3 nm, 6 nm and 11 nm NLs compared with the as-grown NLs in Figure 2.

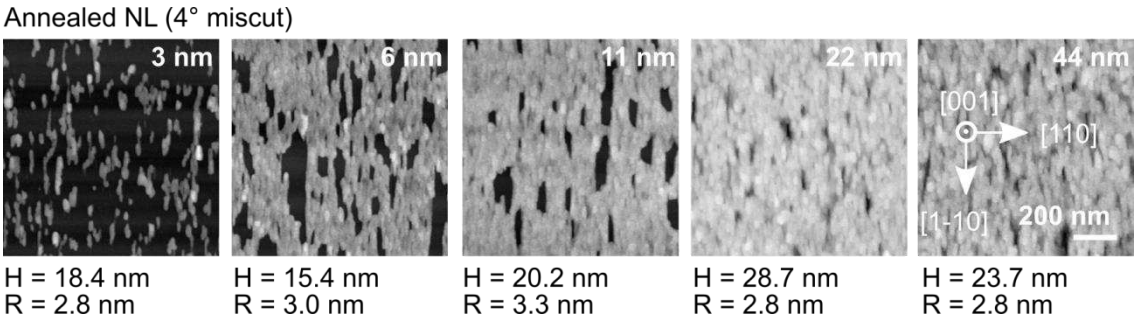

Figure 4 AFM height scans of the set of annealed GaN NLs with different thicknesses revealing the surface morphology. The height (H) and roughness (R) are stated below each AFM scan.

The feature sizes in the [110] and [1-10] directions of the annealed set of NLs grown on the 4° and 2° miscut substrate were quantified using the 2D-FFT method, as shown in Figure 5 (a).

From the AFM scans, the surfaces of the 6 nm and 11 nm thick annealed NLs have a number of pits. This has resulted in the feature size obtained by the 2D-FFT method to be reflective of the size of the pits, rather than of the surface features. Hence the data points for 6 nm and 11 nm thick annealed NLs (within the dashed rectangle) should not be compared directly with the other data points in Figure 5 (a). The feature size in the [110] direction, $f_{[110]}$, increases slightly with increasing NL thickness, while in the [1-10] direction, $f_{[1\text{-}10]}$ does not differ significantly with NL thickness. Similar to the as-grown NLs, the data indicates that miscut does not have an influence on feature size. The aspect ratio ($f_{[1\text{-}10]}$/ $f_{[110]}$) of the features for the as-grown and annealed NLs grown on the 4° and 2° miscut substrates is plotted in Figure 5 (b). The data points for 6 nm and 11 nm thick NLs have been taken out since $f_{[1\text{-}10]}$ and $f_{[110]}$ obtained from the 2D-FFT method do not reflect the actual feature sizes. There is a significant increase in the aspect ratio by a factor of 1.2 to 2 upon annealing, due to a larger increase in the feature size along [1-10] than [110], suggesting that the diffusion constants are anisotropic and higher along the [1-10] direction than the [110] direction.

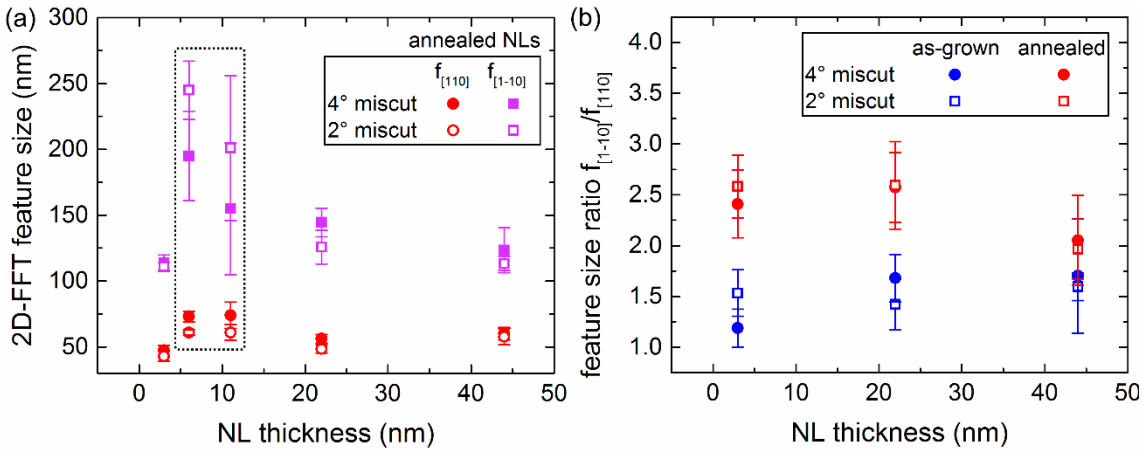

Figure 5 (a) Feature sizes of the annealed NLs grown on 4° (filled) and 2° (open) miscut substrates in the [110] (circle) and [1-10] (square) directions. The data points within the dashed rectangle are from samples where the 2D-FFT feature size measured reflects the sizes of the pits, and hence should not be compared directly with the other data points. (b)

Variation of the aspect ratio of surface features with NL thickness for as-grown (blue) and annealed (red) NLs grown on 4° (filled) and 2° (open) miscut substrates.

Figure 6 shows the AFM scans of two annealed NLs that are (a) 3 nm and (b) 22 nm thick, and both grown on a 2° miscut substrate with the presence of antiphase domains, where neighbouring domains have surface features that are aligned along two perpendicular <110> directions. The anisotropic surface features are observed in both types of domains, and the elongation of the features is assumed to be along the potential valleys of each type of domain. This, together with the AFM scans in Figure 2 and Figure 4, demonstrate that the anisotropy of surface morphology starts at the nucleation stage. As with the surface morphology of the thicker epilayers we have previously studied [26], we suggest that this relates to anisotropic diffusion lengths related to the crystallography of (001) zb-GaN, and in the case of these nucleation layers, possibly similar anisotropy in diffusion of Ga and N adatoms over the (001) 3C-SiC surface which templates the GaN growth.

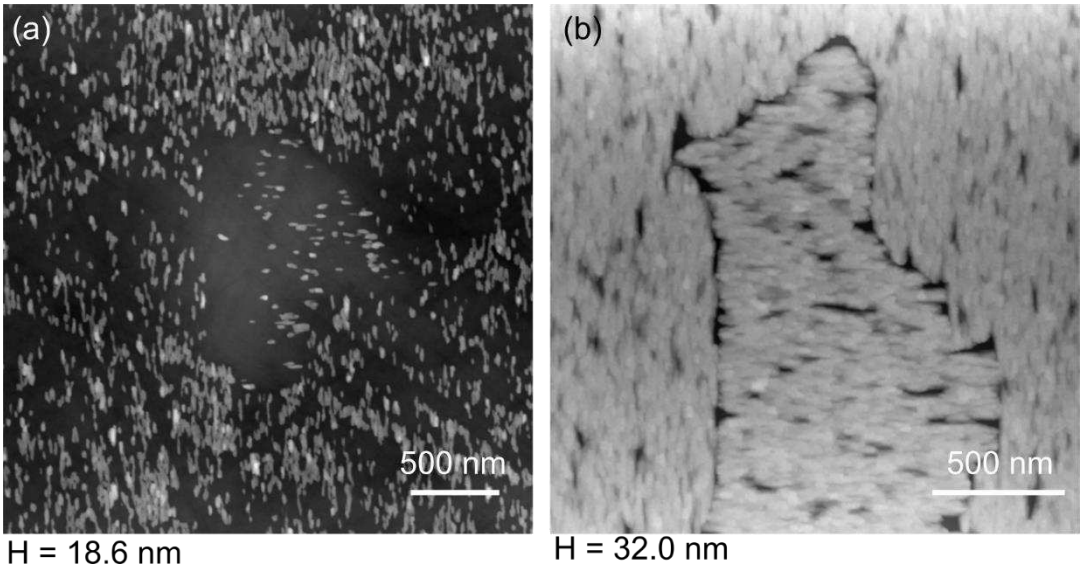

Figure 6 AFM height scans of annealed zb-GaN NL that are (a) 3 nm and (b) 22 nm thick, and grown on a 2° miscut substrate with antiphase domains. The height (h) is shown below each AFM scan.

The coverage of the substrate by the NLs was determined quantitatively from 500 × 500 nm^2 AFM scans for both the as-grown and annealed series of NLs grown on the 4° miscut substrate, as presented in Figure 7 (a). For the as-grown NLs, the SiC substrate is > 94 % covered by GaN even for a nominal thickness of 3 nm, and becomes fully covered (> 99 %) for thicknesses > 6 nm. Despite the reduced coverage at low thickness after the anneal treatment, the substrate coverage increases as the NL thickness is increased from 3 to 22 nm, at which point the substrate again becomes almost completely covered (> 99%).

The surface coverage observations by AFM is in agreement with XRD results from $\omega 2\theta$-scans of the 002 reflections. In Figure 7 (b), the integrated intensity of zb-GaN reflection relative to the 3C-SiC substrate reflection is plotted against NL thickness for both the as-grown and annealed set of NLs. The 3C-SiC substrate reflections are used to normalise the small experimental variations between the measurements of different samples. As the

integrated intensity is proportional to the material volume of a thin sample [25], the ratio of the integrated intensities of the GaN/SiC reflections increases linearly with NL thickness, since there is an increasing volume of GaN deposited. It should be noted that if the data in Figure 7 (b) for the as-grown nucleation layer were extrapolated back to a nominal nucleation layer thickness of zero, this would not correspond to a zero intensity ratio. This implies that there are some small errors in the absolute values presented here, but they should not affect the comparison between the as-grown and annealed samples, which is the key aspect of this analysis. The annealed NLs show a decrease in intensity compared with the as-grown NLs of similar nominal thickness, revealing that material loss occurs during high temperature annealing. This material loss is relatively small and approximately the same for the thicker NL samples, suggesting that the degree of desorption is not as significant for thicker NLs. However, the material loss is large for the thinnest NL of 3 nm thickness, with a relative loss of 73% according to XRD, which fits well with the observation by AFM showing a relative reduction in the surface coverage of the same order (see Figure 7 (a)). Annealing of thinner NLs might result in more material desorption than thicker NLs because the former have less substrate coverage and the islands are not fully coalesced before annealing, hence the NL islands provide a larger surface area and sites for material desorption to take place.

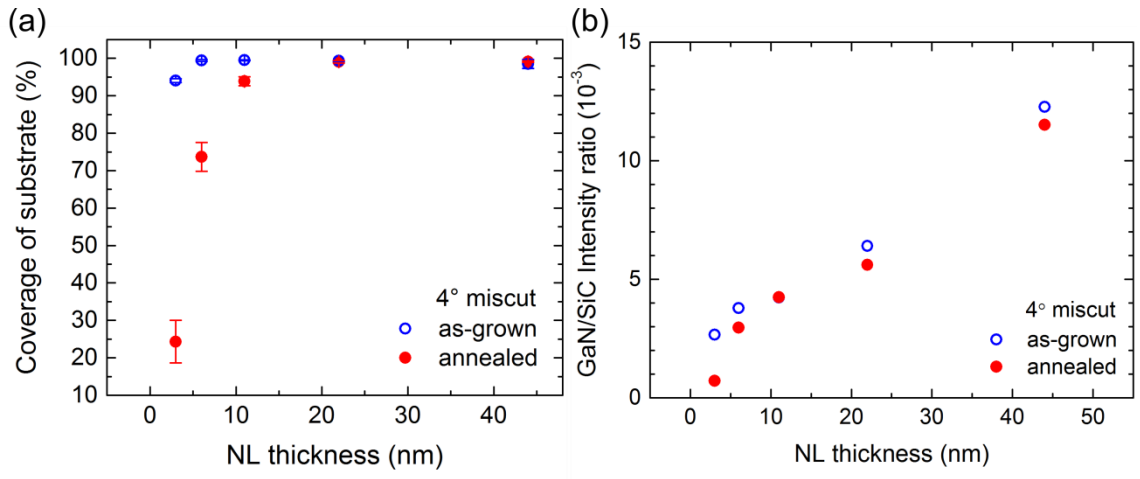

Figure 7 (a) Substrate coverage from AFM measurements and (b) ratio of integrated intensities of the 002 GaN and 3C-SiC reflections from XRD $\omega 2\theta$-scans as function of the nominal NL thickness for the as-grown and annealed sets of NLs grown on the 4° miscut substrate.

To investigate the strain states of the NLs, the intensity profiles of the XRD $\omega 2\theta$-scans of the 002 reflections for the annealed set of NLs grown on the 4° miscut substrate are compared in Figure 8 (a). The X-ray peaks of the thinnest GaN NLs are at lower Bragg angles than the Bragg angle of nominally unstrained zincblende GaN, which is indicated by the dotted line at $2\theta = 39.9845(35)°$. This shows that the GaN nucleation layers are stretched in the growth direction and hence compressed parallel to the interface with SiC. With increasing NL thickness, the integrated intensity of zb-GaN reflection increases and the zb-GaN reflection steadily shifts towards higher Bragg angles, until it reaches the position of relaxed zb-GaN for a NL thickness of 44 nm. The bi-axial in-plane strain in Figure 8 (b) calculated from the peak positions of zb-GaN in the $\omega 2\theta$-scans show that for both as-grown and annealed samples, the compressive in-plane strain reduces in magnitude with increasing thickness, from ~ -2×10^{-2} for the 3 nm thick NL to close to zero for the 44 nm thick NL. The thin NLs are compressively strained to the substrate as zb-GaN has a larger lattice constant than 3C-

SiC, and zb-GaN tries to match the lattice constant of SiC through elastic deformation. As the NL thickness increases, there is more plastic relaxation to result in a decrease in magnitude of the compressive in-plane strains.

It can also be seen from Figure 8 (b) that the annealed NLs (filled circles) have a slightly smaller compressive in-plane strain than the as-grown NLs of similar thickness (open circles), even when the error bars are considered. This suggests that the anneal treatment results in relaxation of the material that is likely related to both the ripening of islands and material desorption, which is seen in the AFM data in Figure 2 and Figure 4, where the islands increase in size while the substrate coverage decreases after the anneal treatment. For 3 nm and 6 nm thick NLs, the annealed samples have significantly smaller compressive in-plane strains than the as-grown NL samples. Due to a low substrate coverage, the islands in the 3 nm and 6 nm annealed NLs may be less constrained parallel to the interface, thus possibly leading to more relaxation and lower in-plane strains.

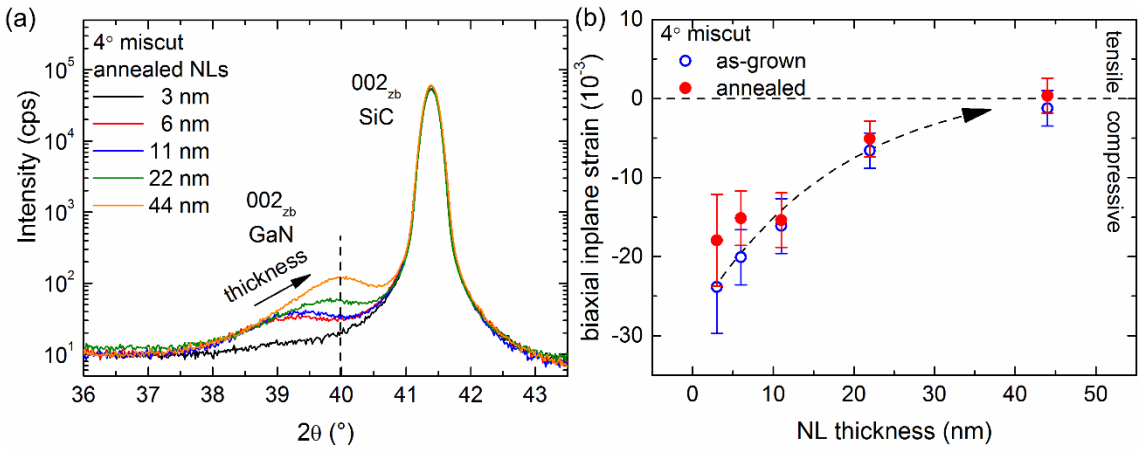

Figure 8 (a) XRD $\omega 2\theta$-scans of the 002 zb-GaN and SiC reflections for the annealed NLs grown on the 4° miscut substrate. The dotted line marks the position of relaxed zb-GaN. (b) The dashed line provides a guide-to-the-eye showing the change in bi-axial in-plane strain

with increasing NL thickness of the as-grown and annealed sets of NLs grown on the 4° miscut substrate.

3.3. HR-STEM characterisation of NLs

HR-STEM images of both the as-grown and annealed NLs show that the layers are of the zincblende phase at the GaN/SiC interface and across the layer. This is in contrast to the growth of wz-GaN on sapphire, where the phase and crystallinity of the as-deposited nucleation layer can change significantly on annealing [30]. An example of a HR-STEM image with zone axis = [-110] of the 22 nm thick annealed NL is shown in Figure 9. This reveals the ABCABC stacking of the {111}-type atomic planes of the zincblende crystal structure (magnified in the inset), and that the atomic stacking is continuous from the SiC substrate to the zb-GaN NL, i.e. without an amorphous layer at the GaN/SiC interface. The blue boxes highlight the stacking faults in the [-110] zone, while the blue circle shows a stacking fault in the [110] zone, which exits at the front and/or back surface of the TEM foil. An extra half-plane from the 3C-SiC layer that terminates in the GaN layer close to the interface with SiC is marked by the red arrow. We attribute the extra half-plane to a misfit dislocation that helps accommodate the lattice mismatch between GaN and SiC. This is consistent with the suggestion that the thicker layers are (at least partially) plastically relaxed, as discussed in the context of the XRD data in Figure 8 (b).

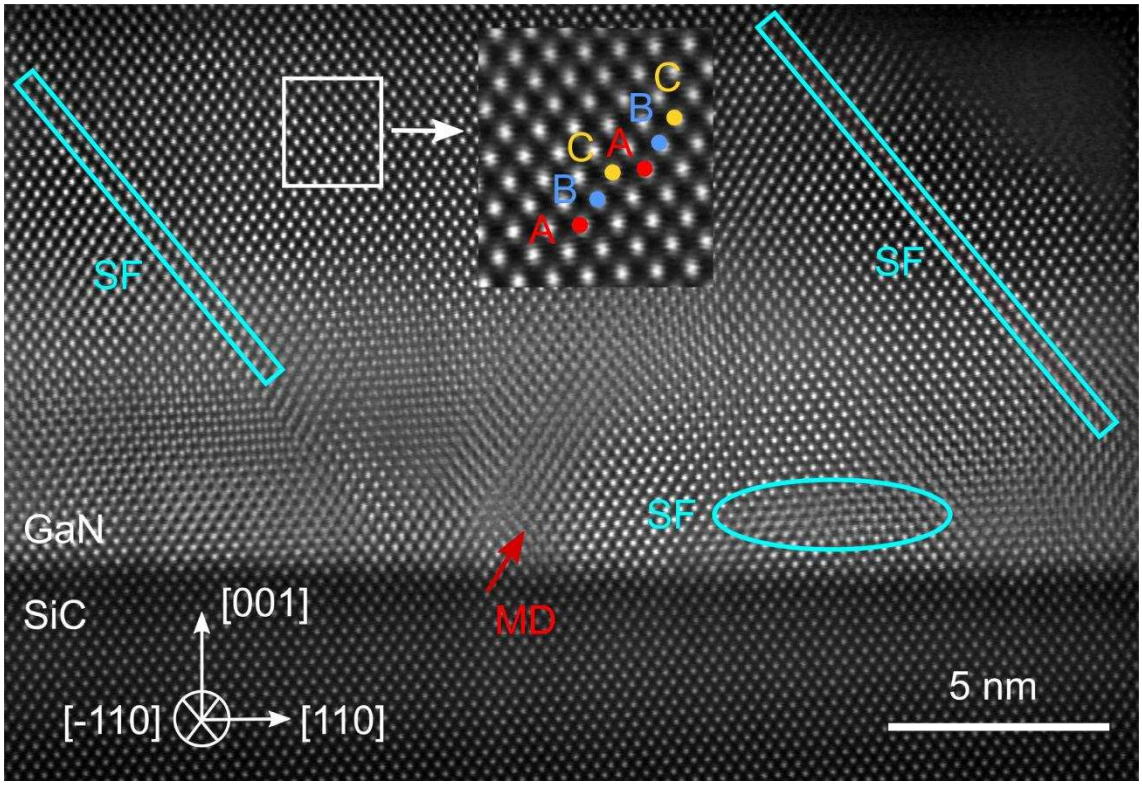

Figure 9 HR-STEM image (zone axis = [-110]) of 22 nm thick annealed NL showing that the NL is fully crystalline with defects present. The ABCABC zincblende stacking is highlighted in the inset which is a magnified image of the area marked by the white box. The blue boxes and circles highlight the stacking faults in the [-110] zone and [110] zone respectively, while the red arrow indicates a misfit dislocation.

3.4. Effect of NL thickness on epilayer growth

Finally, we explore the properties of zb-GaN epilayers grown on the NLs with different thicknesses. Nomarski optical micrographs of the zb-GaN epilayers grown on the various NLs in Figure 10 (a) show that all the epilayers have a surface morphology with elongated features along the [1-10] direction, but the surface of the epilayer grown on the 3 nm thick NL has pits. Moreover, the phase purity analysis from XRD in Figure 10 (b) reveals that the epilayer grown on the 3 nm NL has the highest wurtzite content compared with thicker NLs. Referring to the AFM scans of the annealed set of NLs in Figure 4 and the substrate

coverages determined from AFM and XRD data in Figure 7, the 3 nm annealed NL has the lowest substrate coverage of 26% of all the samples in the series. Therefore, we can conclude that an epilayer grown on NLs with a low substrate coverage of below at least 26% results in a pitted surface and a reduced zincblende phase purity. These results are consistent with the work by Xu *et al.* [22] which concluded that the wurtzite content of the zb-GaN epilayer increased if the substrate coverage of the annealed NL was incomplete. The authors did not specify the NL thickness so a more detailed comparison with our work cannot be made. In contrast, Wu *et al.* [21] reported the growth of an uncoalesced GaN film with a 50% wurtzite content on a 20 nm-thick NL, whereas for the growth method applied here, a NL as thin as 6 nm provides sufficient substrate coverage for zb-GaN epilayer growth with a high phase purity.

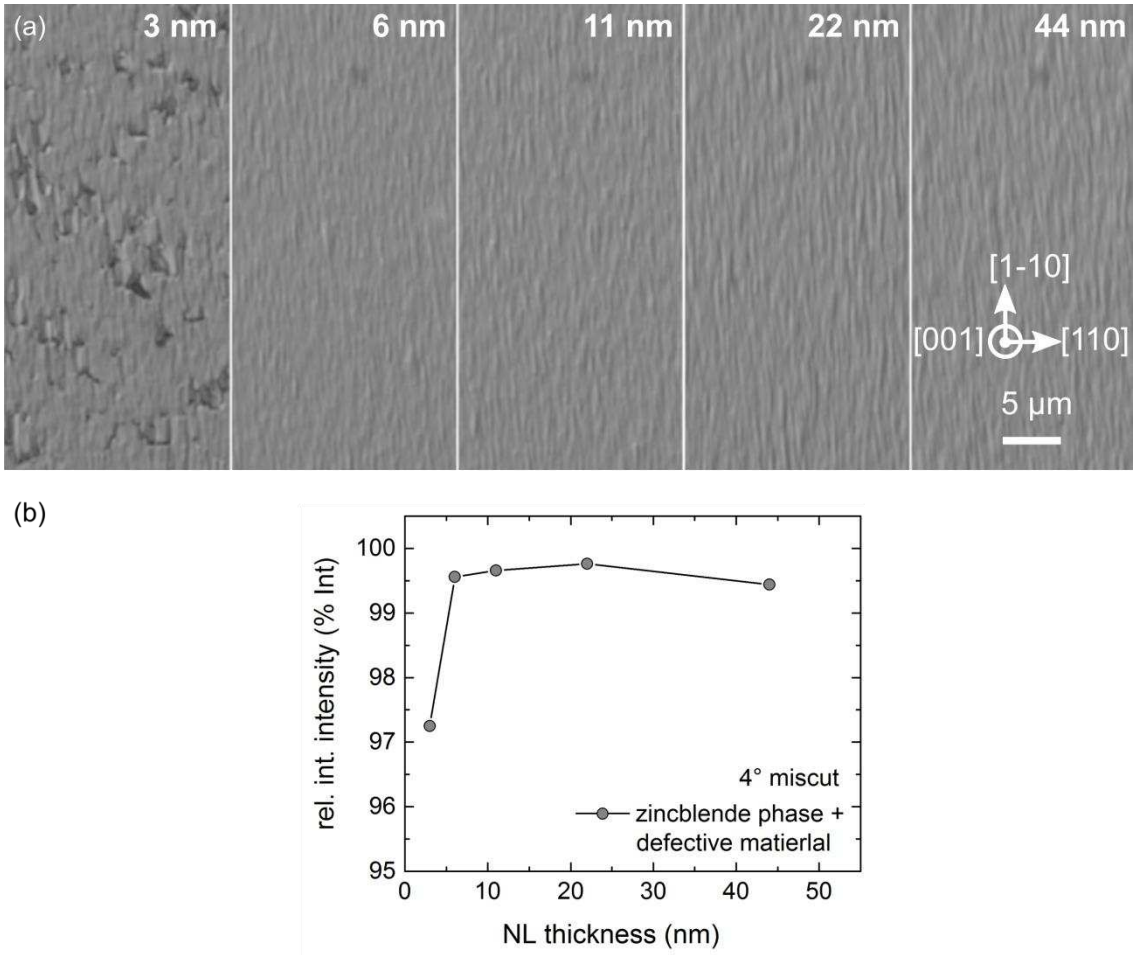

Figure 10 (a) Normarski images of the GaN epilayers grown on NLs with different thicknesses. (b) The sum of the relative integrated intensity of zincblende phase and defective material peaks in the zb-GaN epilayers grown on NLs with different thicknesses, as determined by XRD.

4. Conclusions

Both as-grown and annealed zb-GaN NLs with nominal thicknesses of 3 nm to 44 nm deposited on 3C-SiC/Si substrates by MOVPE are crystalline, have high zincblende phase purity, and contain defects including stacking faults and misfit dislocations. The miscut angle of the substrate (4° versus 2°) does not have an effect on the surface morphology of the NLs. The annealing treatment of the NLs to the higher epilayer growth temperature reduces the substrate coverage, especially for the thinnest layers, due to material desorption and the

ripening of islands. For full coverage (> 99 %) of the substrate, the nominal thickness of the annealed NLs should be at least 22 nm. The substrate coverage of the NL is an important consideration as an incomplete coverage of the 3 nm thick annealed NL resulted in the subsequent epilayer having a pitted surface and a reduced zincblende phase purity. The minimum nominal NL thickness for the growth of zb-GaN films with high phase purity is 6 nm. The compressive bi-axial in-plane strain in the NLs reduces with increasing NL thickness (likely to arise from more plastic relaxation by misfit dislocations and partial dislocations bounding stacking faults), and after the anneal treatment due to relaxation from island ripening and material desorption. In light of such results, we recommend an optimal nominal NL thickness of 22 nm. Lastly, the study confirms that the anisotropy of surface morphology previously observed in zb-GaN epilayers starts at the nucleation stage and is controlled by the crystallography of the top monolayer of the (001) GaN lattice.

Acknowledgements

We would like to thank Innovate UK for the financial support within the Energy Catalyst Round 4 - Mid Stage Feasibility scheme (Ref. 102766), and EPSRC for support through grant no. EP/M010589/1 and grant no. EP/R01146X/1. P Vacek would like to thank the Ministry of Education, Youth and Sports of the Czech Republic for supporting a 6-month research stay at the Cambridge Centre for Gallium Nitride through the project no. CZ.02.2.69/0.0/0.0/16_027/0008056. DJ Wallis would like to acknowledge support from EPSRC Manufacturing fellowship, EP/N01202X/2.

Declarations of interest: none

References

[1] J. Schörmann, D.J. As, K. Lischka, P. Schley, R. Goldhahn, S.F. Li, W. Löffler, M. Hetterich, H. Kalt, Molecular beam epitaxy of phase pure cubic InN, Appl. Phys. Lett. 89 (2006) 2004–2007. doi:10.1063/1.2422913.

[2] D.J. As, Cubic group-III nitride-based nanostructures — basics and applications in optoelectronics, Microelectronics J. 40 (2009) 204–209. doi:10.1016/j.mejo.2008.07.036.

[3] I. Vurgaftman, J.R. Meyer, Band parameters for nitrogen-containing semiconductors, J. Appl. Phys. 94 (2003) 3675–3696. doi:10.1063/1.1600519.

[4] M.J. Paisley, Z. Sitar, J.B. Posthill, R.F. Davis, Growth of cubic phase gallium nitride by modified molecular-beam epitaxy, J. Vac. Sci. Technol. A. 7 (1989) 701. doi:10.1116/1.575869.

[5] S. Strite, J. Ruan, Z. Li, A. Salvador, H. Chen, D.J. Smith, W.J. Choyke, H. Morkoç, An investigation of the properties of cubic GaN grown on GaAs by plasma-assisted molecular-beam epitaxy, J. Vac. Sci. Technol. B. 9 (1991) 1924–1929. doi:10.1116/1.585381.

[6] O. Brandt, H. Yang, B. Jenichen, Y. Suzuki, L. Däweritz, K.H. Ploog, Surface reconstructions of zinc-blende GaN/GaAs(001) in plasma-assisted molecular-beam epitaxy, Phys. Rev. B. 52 (1995) R2253.

[7] D. Schikora, M. Hankeln, D.J. As, K. Lischka, T. Litz, A. Waag, T. Buhrow, F. Henneberger, Epitaxial growth and optical transitions of cubic GaN films, Phys. Rev. B. 54 (1996) R8381–R8384. doi:10.1103/PhysRevB.54.R8381.

[8] H. Okumura, K. Ohta, G. Feuillet, K. Balakrishnan, S. Chichibu, H. Hamaguchi, P. Hacke, S. Yoshida, Growth and characterization of cubic GaN, J. Cryst. Growth. 178

(1997) 113. doi:10.1016/S0022-0248(97)00084-5.

[9] A. Trampert, O. Brandt, H. Yang, K.H. Ploog, Direct observation of the initial nucleation and epitaxial growth of metastable cubic GaN on (001) GaAs, Appl. Phys. Lett. 70 (1997) 583–585. doi:10.1063/1.118281.

[10] B. Daudin, G. Feuillet, J. Hübner, Y. Samson, F. Widmann, A. Philippe, C. Bru-Chevallier, G. Guillot, E. Bustarret, G. Bentoumi, A. Deneuville, How to grow cubic GaN with low hexagonal phase content on (001) SiC by molecular beam epitaxy, J. Appl. Phys. 84 (1998) 2295–2300. doi:10.1063/1.368296.

[11] D.J. As, A. Richter, J. Busch, M. Lübbers, J. Mimkes, K. Lischka, Electroluminescence of a cubic GaN/GaAs (001) p–n junction, Appl. Phys. Lett. 76 (2000) 13. doi:10.1063/1.125640.

[12] E. Martinez-Guerrero, E. Bellet-Amalric, L. Martinet, G. Feuillet, B. Daudin, H. Mariette, P. Holliger, C. Dubois, C. Bru-Chevallier, P. Aboughe Nze, T. Chassagne, G. Ferro, Y. Monteil, Structural properties of undoped and doped cubic GaN grown on SiC(001), J. Appl. Phys. 91 (2002) 4983–4987. doi:10.1063/1.1456243.

[13] D.J. As, D. Schikora, K. Lischka, Molecular beam epitaxy of cubic III-nitrides on GaAs substrates, Phys. Status Solidi C. 0 (2003) 1607–1626. doi:10.1002/pssc.200303133.

[14] B.M. Shi, M.H. Xie, H.S. Wu, N. Wang, S.Y. Tong, Transition between wurtzite and zinc-blende GaN: An effect of deposition condition of molecular-beam epitaxy, Appl. Phys. Lett. 89 (2006) 151921. doi:10.1063/1.2360916.

[15] D.J. As, R. Kemper, C. Mietze, T. Wecker, J.K.N. Lindner, P. Veit, A. Dempewolf, F. Bertram, J. Christen, Spatially resolved optical emission of cubic GaN/AlN multi-quantum well structures, Mater. Res. Soc. Symp. Proc. 1736 (2014).

doi:10.1557/opl.2014.944.

[16] A. Nakadaira, H. Tanaka, Growth of zinc-blende GaN on GaAs (100) substrates at high temperature using low-pressure MOVPE with a low V/lll molar ratio, J. Electron. Mater. 26 (1997) 320–324. doi:10.1007/s11664-997-0171-z.

[17] J. Wu, H. Yaguchi, H. Nagasawa, Y. Yamaguchi, K. Onabe, Y. Shiraki, R. Ito, Crystal structure of GaN grown on 3C-SiC substrates by metalorganic vapor phase epitaxy, Jpn. J. Appl. Phys. 36 (1997) 4241–4245. doi:10.1143/JJAP.36.4241.

[18] J. Wu, H. Yaguchi, K. Onabe, R. Ito, Y. Shiraki, Photoluminescence properties of cubic GaN grown on GaAs(100) substrates by metalorganic vapor phase epitaxy, Appl. Phys. Lett. 71 (1997) 2067. doi:10.1063/1.119344.

[19] J. Wu, H. Yaguchi, K. Onabe, Y. Shiraki, R. Ito, Metalorganic vapor phase epitaxy growth of high quality cubic GaN on GaAs (100) substrates, Jpn. J. Appl. Phys. 37 (1998) 1440–1442. doi:10.1143/JJAP.37.1440.

[20] J. Camassel, P. Vicente, N. Planes, J. Allegre, J. Pankove, F. Namavar, Experimental investigation of cubic to hexagonal ratio for GaN layers deposited on 3C-SiC/Si, Phys. Status Solidi B. 216 (1999) 253–257.

[21] J. Wu, H. Yaguchi, B.P. Zhang, Y. Segawa, K. Onabe, Y. Shiraki, Optical Properties of Cubic GaN Grown on 3C-SiC (100) Substrates by Metalorganic Vapor Phase Epitaxy, Phys. Status Solidi A. 180 (2000) 403–407. doi:10.1002/1521-396X(200007)180:1<403::AID-PSSA403>3.0.CO;2-A.

[22] D. Xu, H. Yang, J.B. Li, S.F. Li, Y.T. Wang, D.G. Zhao, R.H. Wu, Initial stages of GaN/GaAs (100) growth by metalorganic chemical vapor deposition, J. Electron. Mater. 29 (2000) 177–182. doi:10.1007/s11664-000-0138-9.

[23] C.H. Wei, Z.Y. Xie, L.Y. Li, Q.M. Yu, J.H. Edgar, MOCVD growth of cubic GaN on

3C-SiC deposited on Si (100) substrates, J. Electron. Mater. 29 (2000) 317–321. doi:10.1007/s11664-000-0070-z.

[24] Z.H. Feng, H. Yang, X.H. Zheng, Y. Fu, Y.P. Sun, X.M. Shen, Y.T. Wang, Optimization of cubic GaN growth by metalorganic chemical vapor deposition based on residual strain relaxation, Appl. Phys. Lett. 82 (2003) 206–208. doi:10.1063/1.1536714.

[25] M. Frentrup, L.Y. Lee, S.-L. Sahonta, M.J. Kappers, F.C.-P. Massabuau, P. Gupta, R.A. Oliver, C.J. Humphreys, D.J. Wallis, X-ray diffraction analysis of cubic zincblende III-nitrides, J. Phys. D. Appl. Phys. 50 (2017) 433002. doi:10.1088/1361-6463/aa865e.

[26] L.Y. Lee, M. Frentrup, M.J. Kappers, R.A. Oliver, C.J. Humphreys, D.J. Wallis, Effect of growth temperature and V/III-ratio on the surface morphology of MOVPE-grown cubic zincblende GaN, J. Appl. Phys. 124 (2018) 105302. doi:10.1063/1.5046801.

[27] I. Horcas, R. Fernández, J.M. Gómez-Rodríguez, J. Colchero, J. Gómez-Herrero, A.M. Baro, WSXM: A software for scanning probe microscopy and a tool for nanotechnology, Rev. Sci. Instrum. 78 (2007) 013705. doi:10.1063/1.2432410.

[28] D. Nečas, P. Klapetek, Gwyddion: an open-source software for SPM data analysis, Cent. Eur. J. Phys. 10 (2012) 181–188. doi:10.2478/s11534-011-0096-2.

[29] U.W. Pohl, Thermodynamics of Epitaxial Layer-Growth, in: Ep. Semicond., Springer-Verlag Berlin Heidelberg, 2013: pp. 154–155.

[30] X.H. Wu, D. Kapolnek, E.J. Tarsa, B. Heying, S. Keller, B.P. Keller, U.K. Mishra, S.P. DenBaars, J.S. Speck, Nucleation layer evolution in metal-organic chemical vapor deposition grown GaN, Appl. Phys. Lett. 68 (1996) 1371–1373. doi:10.1063/1.116083.